The Astrophysical Journal Letters, 866:L5 (8pp), 2018 October 10 https://doi.org/10.3847/2041-8213/aae377

Redshift Evolution of the Black Hole Merger Rate from Globular Clusters

Carl L. Rodriguez[1,3] and Abraham Loeb[2]
[1] MIT-Kavli Institute for Astrophysics and Space Research, 77 Massachusetts Avenue, 37-664H, Cambridge, MA 02139, USA
[2] Astronomy Department, Harvard University, 60 Garden Street, Cambridge, MA 02138, USA
Received 2018 August 24; revised 2018 September 14; accepted 2018 September 21; published 2018 October 4

Abstract

As the sensitivity of current and future gravitational-wave detectors improves, it will become possible to measure the evolution of the binary black hole merger rate with redshift. Here, we combine detailed fits to state-of-the-art dynamical models of binary black hole formation in dense star clusters with a cosmological model of cluster formation across cosmic time. We find a typical merger rate of $14\,\mathrm{Gpc^{-3}\,yr^{-1}}$ in the local universe, with a reasonable range of 4–$18\,\mathrm{Gpc^{-3}\,yr^{-1}}$, depending on the rate of cluster disruption and the cluster initial mass function. This rate increases by a factor of 6 to redshift $z = 2.7$ before declining at higher redshifts. We compare the merger rate from binaries produced in clusters to similar estimates from isolated binaries and triples in galactic fields, and discuss various ways that these different formation channels could add up to the current merger rate observed by the Laser Interferometer Gravitational-Wave Observatory/Virgo.

Key words: globular clusters: general – gravitational waves – stars: black holes

1. Introduction

The detection of gravitational waves (GWs) from merging binary black holes (BBHs) by the Advanced Laser Interferometer Gravitational-Wave Observatory (LIGO)/Virgo (Abbott et al. 2017c, 2017b, 2017d, 2016a, 2016b) has stimulated many theoretical questions about their origin. While a rich variety of formation channels have been proposed to explain these events, the vast majority fall into one of two categories. In the first, the BBHs are formed as the end-stage of evolution for a massive binary, and merge through the emission of GWs either following a common-envelope phase (the "field" channel, e.g., Belczynski et al. 2002, 2010, 2016; Podsiadlowski et al. 2003; Voss & Tauris 2003; Sadowski et al. 2008; Dominik et al. 2012, 2013, 2015), or by secular interaction with a third companion (the "triple" channel, e.g., Antonini & Perets 2012; Antonini et al. 2016, 2017; VanLandingham et al. 2016; Petrovich & Antonini 2017; Silsbee & Tremaine 2017; Hoang et al. 2018; Leigh et al. 2018; Rodriguez & Antonini 2018). In the second category, BBHs are dynamically forged through two- or three-body encounters in dense stellar environments such as globular clusters (GCs) or galactic nuclei (e.g., Portegies Zwart & Mcmillan 2000; O'Leary et al. 2006, 2007; Moody & Sigurdsson 2009; Banerjee et al. 2010; Downing et al. 2010, 2011; Tanikawa 2013; Bae et al. 2014; Ziosi et al. 2014; Rodriguez et al. 2015, 2016a, 2016b, 2018; Askar et al. 2016; Banerjee 2017; Giesler et al. 2018).

While any of these formation channels can produce BBH mergers with masses and spins similar to those observed by LIGO/Virgo, the physical processes that drive BBHs to merge operate on significantly different timescales in each channel. Even though the majority of these mechanisms are modulated by the same cosmic star formation rate (SFR), the different delay times between BBH formation and merger will produce different merger rate distributions in each over redshift. These differences may be detectable by either the current (Fishbach et al. 2018) or future (Hild et al. 2011; Abbott et al. 2017a; Vitale & Farr 2018) generation of GW detectors, and can be used to disentangle the contributions of different formation channels to the overall BBH merger rate.

In this Letter, we use state-of-the-art dynamical models of GCs from Rodriguez et al. (2018) and a detailed model of GC formation across cosmic time (El-Badry et al. 2018) to compute a cosmological rate of BBH mergers from the dynamical channel. Unlike previous calculations (Portegies Zwart & Mcmillan 2000; Askar et al. 2016; Rodriguez et al. 2016a), this calculation allows us to directly compare the evolution of the dynamical BBH merger rate to that from other channels shaped by the cosmic SFR, such as the classical field channel (taken from Belczynski et al. 2016) and the field triple channel (taken from Rodriguez & Antonini 2018).

In Section 2, we describe the details of our dynamical GC models, and how we use the GC formation model of El-Badry et al. (2018) to compute the BBH merger rate. In Section 3, we explore the evolution of the merger rates over redshift, and show how our model depends on assumptions about GC disruption and the cluster initial mass function (CIMF). Finally, in Section 4, we compare the cosmic merger rates from GCs to those from isolated binaries and from stellar triples, and show how the current LIGO/Virgo merger rates can be explained by different combinations of the three different formation channels. Throughout this Letter, we assume a ΛCDM cosmology with $h = 0.679$ and $\Omega_M = 0.3065$ (Ade et al. 2016).

2. Rate Fits

El-Badry et al. (2018) have developed a formalism to model the formation of GCs by populating galaxy halos with GCs based on gas mass and pressure, while tracking the fate of these GCs during the merger assembly history of their host galaxies. To get the formation of GCs in different halo masses across cosmic time, we created phenomenological fits to their total SFR in GCs per comoving volume per halo mass at a given redshift. We followed their "standard" model, but included the additional factor of 2.6 in their α_Γ parameter to account for cluster disruption (see Appendix A). To translate this into a rate of BBH mergers, we need only to convolve this cosmological

[3] Pappalardo Fellow.

cluster SFR with the rate of BBH mergers from GCs. Our rate equation for the merger rate of BBHs at a cosmic time t is

$$\mathcal{R}(t) = \iiint \frac{\dot{M}_{\rm GC}}{d\log_{10}M_{\rm Halo}}\Bigg|_{z(\tau)} \frac{1}{\langle M_{\rm GC}\rangle} P(M_{\rm GC}) \times R(r_v, M_{\rm GC}, \tau - t)\, dM_{\rm Halo}\, dM_{\rm GC}\, d\tau, \quad (1)$$

where $\frac{\dot{M}_{\rm GC}}{d\log_{10}M_{\rm Halo}}$ is the comoving rate of star formation in GCs (in units of $M_\odot\,{\rm yr}^{-1}\,{\rm Mpc}^{-3}$) per galaxies of a given halo mass $M_{\rm Halo}$ at a redshift $z(\tau)$ corresponding to a formation time τ. $P(M_{\rm GC})$ is the CIMF, which we take to be $\propto M_{\rm GC}^{-2}$ between $10^5\,M_\odot$ and $10^7\,M_\odot$ (though we explore variations to this in Section 3). $\langle M_{\rm GC}\rangle$ is the mean initial mass of a GC given our assumed CIMF. This converts the mass that goes into forming GCs into the number of GCs formed. Finally, $R(r_v, M_{\rm GC}, t)$ is the rate of mergers (ejected and in-cluster) for a GC with a given initial virial radius r_v and mass $M_{\rm GC}$ at a time t after its formation.

For our merger rate from individual clusters, there are two different effects that must be considered. First, as noted in Rodriguez et al. (2016a), the dependence of the BBH merger rate on cluster mass is super-linear. While the number of BHs in any given cluster scales linearly with the cluster mass, the fraction of BBHs that will merge in a Hubble time also increases with the mass of the cluster. This occurs because a more massive cluster forms BBHs in a deeper potential well, requiring more scattering encounters to harden the binary until its inevitable ejection or merger. At the same time, as the cluster loses mass and expands over time, the rates of BBH hardening and ejection will decrease. This causes the BBH merger rate to decrease exponentially over time (e.g., Tanikawa 2013; Hong et al. 2018). Combining these different physical intuitions, we find that the following phenomenological rate formula provides a good fit to the BBH merger rate of individual cluster

$$R(M_{\rm GC}, t) \equiv (AM_{\rm GC}^2 + BM_{\rm GC} + C) \times t^{-(\gamma+\gamma_M \log_{10} M_{\rm GC})} \quad (2)$$

where $M_{\rm GC}$ is the initial cluster mass and t is the age of the given cluster. As the models from Rodriguez et al. (2018) only cover two virial radii (1 and 2 pc), we do not attempt to incorporate this information in our fit (though see Choksi et al. 2018; Hong et al. 2018, for an exploration of the parameter space of cluster initial radii). Instead, we separately fit (2) to all of the models with $r_v = 1$ pc and $r_v = 2$ pc. In reality, our model should incorporate information about the virial radius in the fit itself (as was done using the central cluster density in Hong et al. 2018), but the separate fits allow us to disentangle the influence of cluster concentration on the redshift distribution of BBH mergers. We also fit separately the in-cluster mergers and those that are ejected from the cluster and merge later, because there is no reason to expect them to follow the same phenomenological fits. This produces four total sets of parameters $\theta = (A, B, C, \gamma, \gamma_M)$. For more details about our fitting procedure, see Appendix B.

3. Cosmological Merger Rates

Figure 1 shows the standard merger rates as a function of redshift using our phenomenological fits and Equation (1). We show separately the in-cluster and ejected mergers for BBHs from clusters with $r_v = 1$ pc and $r_v = 2$ pc. In all four cases, the merger rate slowly increases as GCs are formed in the early universe. The in-cluster mergers peak at $z \sim 3$ ($z \sim 2.6$) for the 1 pc (2 pc) clusters, while the ejected mergers peak later at $z \sim 2.3$ ($z \sim 2$). This delay is expected: in-cluster mergers are prompt mergers, occurring almost immediately after the last dynamical encounter in the cluster. Ejected mergers, on the other hand, can sometimes experience a significant delay between their ejection and subsequent merger (as long as 10 Gyr, see Rodriguez et al. 2016b). At the same time, clusters with larger virial radii have correspondingly longer half-mass relaxation times ($\propto r_v^{3/2}$). The time for the BHs to segregate near the cluster center also scales as the half-mass relaxation time of the cluster, so GCs with larger virial radii will require more time to dynamically form BBHs; this, in turn, produces a lag in both the ejected and in-cluster mergers.

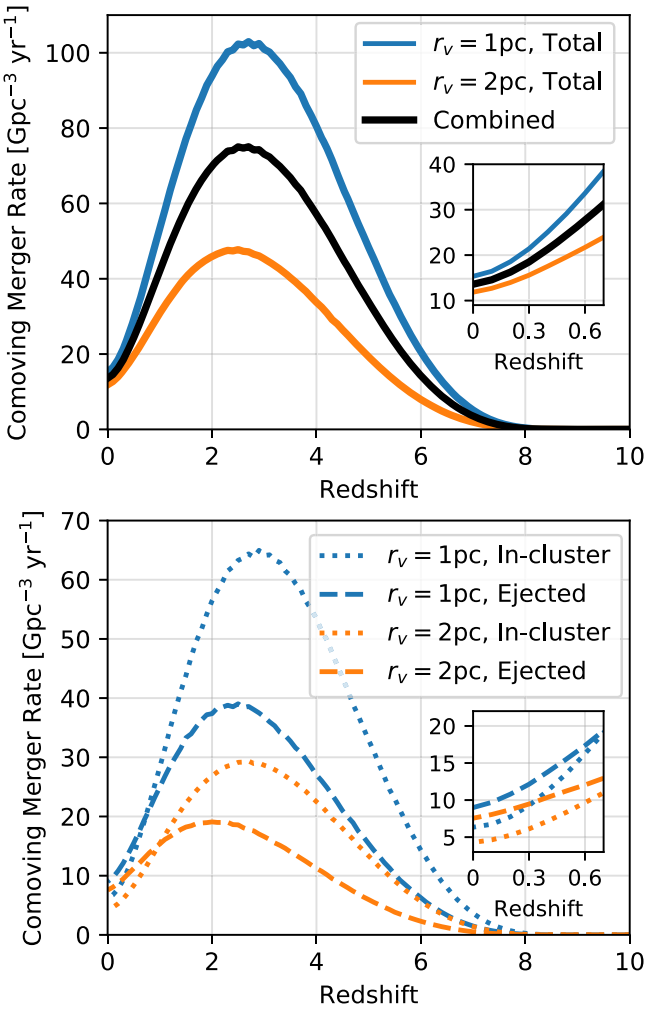

Figure 1. Comoving merger rates of BBHs from GCs in our standard model. We show separately the evolution of the in-cluster and ejected BBH mergers and models with initial virial radii of 1 and 2 pc. Our fiducial model assumes 50% of clusters form with $r_v = 1$ pc and 50% form with $r_v = 2$ pc.

At early times, the in-cluster mergers dominate the BBH merger rates, with the 1 pc models predicting a maximum in-cluster merger rate of $\gtrsim 60\,{\rm Gpc}^{-3}\,{\rm yr}^{-1}$ at $z \sim 3$. However, the delay time between formation and merger for the ejected BBHs shifts the distribution toward lower redshifts, such that at late times the rate of ejected BBHs is nearly twice that of the

in-cluster mergers. For the 1 pc mergers, the ejected mergers become dominant at $z \lesssim 0.7$, which increases to $z \lesssim 0.9$ for the 2 pc mergers. The total merger rate from our models in the local universe ($z \lesssim 0.1$) is 15 $\mathrm{Gpc^{-3}\,yr^{-1}}$ for GCs with $r_v = 1$ pc and 12 $\mathrm{Gpc^{-3}\,yr^{-1}}$ for $r_v = 2$ pc.

As a general trend, a larger virial radius decreases the overall merger rate, but increases the delay between BBH formation and merger, flattening the distribution in the local universe. This trend has been independently shown by Choksi et al. (2018), which used semi-analytic models of BBH mergers from GCs to fully explore the parameter space of initial conditions. To limit our computational requirements, we have assumed virial radii of 1 and 2 pc because this brackets the observed peak of effective radii for star formation in the local universe (e.g., Scheepmaker et al. 2007). Furthermore, recent theoretical work (Kremer et al. 2018) has shown that very compact initial radii are required to eject the majority of BHs in any given GC, which necessary to reproduce the observed surface brightness profiles of core-collapsed clusters. For the remainder of this Letter, we will assume a standard model where 50% of clusters form with $r_v = 1$ pc and 50% form with $r_v = 2$ pc. This yields a local merger rate of 14 $\mathrm{Gpc^{-3}\,yr^{-1}}$, where the ejected mergers become dominant for $z \lesssim 0.8$.

3.1. Variations of the CIMF

As in El-Badry et al. (2018), we have assumed that the GC initial mass function follows a simple $M_{\rm GC}^{-2}$ distribution from 10^5 to $10^7\,M_\odot$. However, there is observational evidence that the CIMF contains an exponential truncation at higher masses, and that the truncation depends on galaxy type (see Portegies Zwart et al. 2010, for a review). This function is often written as

$$\phi(M_{\rm GC})dM_{\rm GC} \propto M_{\rm GC}^{-2}\exp(-M_{\rm GC}/M_{\rm GC}^{\star})dM_{\rm GC}, \quad (3)$$

where $M_{\rm GC}^{\star}$ is the truncation mass.

To test the influence of the CIMF on our present estimate, we recompute Equation (1) with $M_{\rm GC}^{\star} = 2 \times 10^5\,M_\odot$ (as suggested by observations for spiral galaxies; Gieles et al. 2006; Larsen 2009) and $M_{\rm GC}^{\star} = 10^6\,M_\odot$ (as suggested by observations for interacting and luminous infrared (IR) galaxies, Bastian 2008). We show the results of these computations in the top panel of Figure 2. Clearly reducing the number of initially massive GCs significantly suppresses the BBH merger rate; even the $M_{\rm GC}^{\star} = 10^6\,M_\odot$ truncation reduces the local merger rate to 6 $\mathrm{Gpc^{-3}\,yr^{-1}}$ while the $2 \times 10^5\,M_\odot$ truncation reduces the local merger rate to 4 $\mathrm{Gpc^{-3}\,yr^{-1}}$. Of course, it is believed that many of these most massive GCs formed many Gyr ago, only to spiral into the center of their respective galaxies due to dynamical friction (e.g., Gnedin & Ostriker 1997). While this would suppress any in-cluster mergers from these clusters at late cosmic times due to tidal disruption, many of the ejected BBHs would remain outside of the disrupting clusters, allowing them to merge many Gyr after their birth clusters have been destroyed. As the mergers of ejected BBHs are the larger contributor to the rates presented here, it is entirely likely that many of the BBHs from these massive clusters will still contribute to the overall merger rate.

To better quantify the contributions from massive GCs to the predicted merger rate, we recompute our standard model using the same $M_{\rm GC}^{-2}$ CIMF, but with progressively decreasing upper limits for the maximum GC mass. This is shown at the bottom of Figure 2. As the upper limit is decreased from 10^7 to $10^6\,M_\odot$, the rate in the local universe decreases roughly linearly from 14 to 5 $\mathrm{Gpc^{-3}\,yr^{-1}}$. Although our analytic model does likely overestimate the number of mergers for the most massive clusters (see Appendix B), we note that these clusters do not dominate the BBH merger rate computed here, ensuring that our results are robust to within a factor of ∼2.

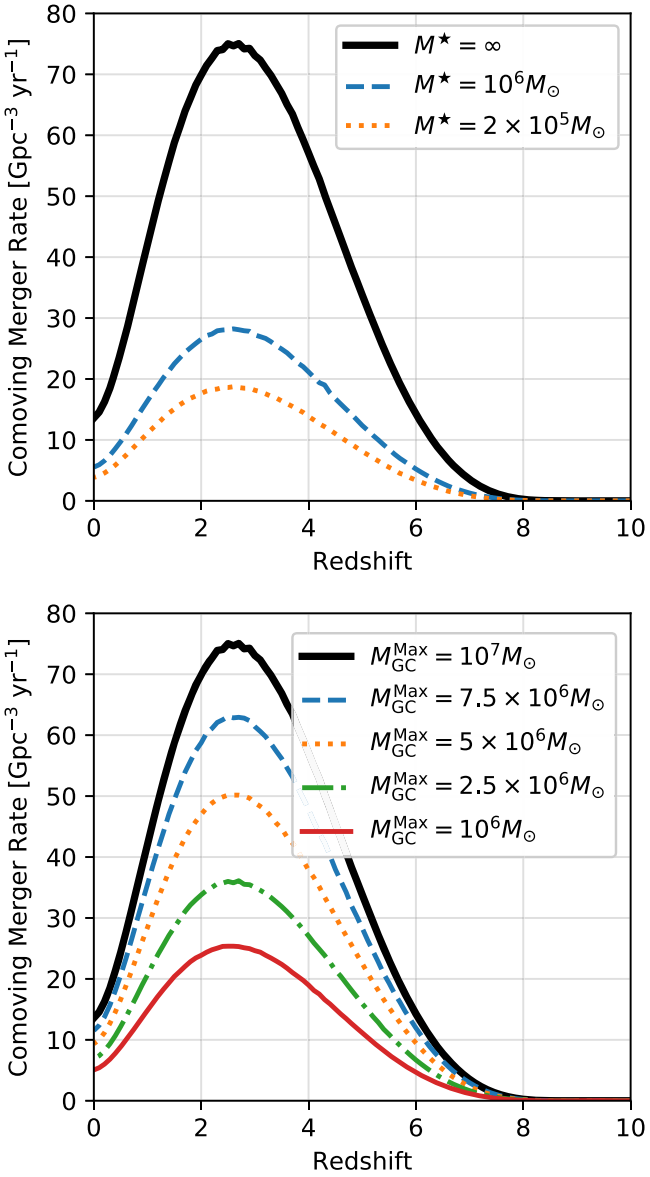

Figure 2. Sensitivity of our result from Equation (1) to the cutoff of the CIMF. In the top panel, we show how the introduction of an exponential truncation in the $M_{\rm GC}^{-2}$ mass function significantly reduces the merger rate. In the bottom panel, we show how the rate reduces as a function of the maximum GC mass at formation.

3.2. Cluster Disruption

We have so far assumed the fiducial model of El-Badry et al. (2018), with an additional multiplicative factor of 2.6 taken from their Appendix D. This additional factor was shown, when combined with the cluster disruption model of Choksi et al. (2018), to reproduce the present-day relationship between galaxy halo mass and GC mass in the local universe (Harris et al. 2014). However, there is still a large amount of

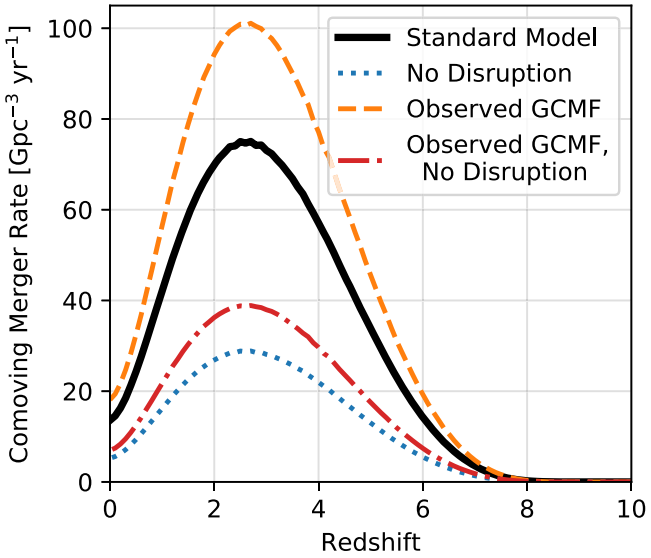

Figure 3. Sensitivity of the BBH merger rate to assumptions about cluster disruption. We show the merger rate computed assuming four different approaches to cluster disruption. In the first two, we assume the standard $\propto M_{\rm GC}^{-2}$ CIMF with no disruption (highly nonphysical), in which all clusters survive for a Hubble time with no mass loss, and our standard model, which includes a correction factor from (El-Badry et al. 2018). We also show the merger rate assuming that GCs form according to the observed GCMF, with and without the correction factor for GC disruption.

uncertainty regarding GC formation and disruption. To attempt to bracket this uncertainty, we perform two additional calculations. In the first, we assume the standard model of El-Badry et al. (2018), but with no cluster disruption (i.e., without the additional factor of 2.6). This model is obviously unphysical, as it allows all low-mass clusters to survive to the present day, whereas in reality such clusters will be destroyed by two-body evaporation or tidal stripping. Because this model significantly underpredicts the number of massive GCs in the local universe, we consider it a highly conservative (if unphysical) lower limit on GC disruption.

For the most optimistic assumption, we instead assume that clusters form according to the observed GC mass function (GCMF). The observed mass distribution of present-day GCs has been shown to follow a roughly log-normal distribution (Harris et al. 2014), assuming a mass-to-light ratio of 2 (Bell et al. 2003), with a peak near $M_{\rm GC}^{\rm peak} = 3 \times 10^5\,M_\odot$. Dynamical modeling of GCs has shown that a typical GC near the peak of the present-day mass function will lose approximately half its mass over 12 Gyr, largely due to stellar evolution, evaporation, and tidal stripping (e.g., Morscher et al. 2015). To that end, we re-integrate Equation (1) using the log-normal luminosity function from Harris et al. (2014), with the median increased by a factor of 4 (to account for both the mass-to-light ratio and the mass loss in an individual GC over $\sim$12 Gyr). This log-normal distribution is representative of GCs that survive disruption, so we consider the GCMF with and without the additional factor of 2.6. When the factor of 2.6 is included, this represented an upper bound on cluster disruption (the observed GCMF has already been shaped by cluster disruption). When it is not included, our model reverts to using the present-day observed population of GCs (as was done in Rodriguez et al. 2016a), albeit with a different distribution of GC formation times.

In Figure 3, we show our fiducal model alongside models with no disruption and disruption around the GCMF. Our model with no disruption only achieves a merger rate of 5 Gpc^{-3} yr^{-1} in the local universe. We reiterate that his model is unrealistic, as it does not include any mass loss or tidal disruption of clusters, but we include it for completeness. Our model pinned to the observed GCMF increases the merger rate by $\sim$40% to 18 Gpc^{-3} yr^{-1} when the additional factor of 2.6 is employed, although we consider this equally unrealistic as it overpredicts the number of massive clusters. Combining this estimate of our most optimistic and realistic assumptions about GC disruption with the smallest estimate from the previous section (where the CIMF was truncated at $M_{\rm GC}^{\star} = 2 \times 10^5\,M_\odot$), we can confidently bracket the merger rate in the local universe as lying between 5 and 18 Gpc^{-3} yr^{-1}, with a reasonable value of 14 Gpc^{-3} yr^{-1}. Finally, the model using the observed GCMF without the disruption correction from El-Badry et al. (2018) yields a local merger rate of 7 Gpc^{-3} yr^{-1}. This assumes that only the present-day population of GCs contribute to the merger rate, similar to the calculation of Rodriguez et al. (2015, 2016a), and yields a similar result (with a small increase arising from the inclusion of post-Newtonian effects and a distribution of cluster formation times).

4. Comparing Different Merger Rates

The fundamental question is whether any of these calculated merger rates can explain the BBH merger rate measured by Advanced LIGO/Virgo. The current limits on the BBH merger rate in the local universe are model dependent and highly sensitive to the assumed black hole (BH) mass distribution. If a model with a uniform logarithmic mass distribution is assumed, then the current observed rates are 32^{+33}_{-22} Gpc^{-3} yr^{-1} in the local universe at the 90% level, fully consistent with the merger rates presented so far. On the other hand, if a power-law BH mass distribution with a slope of $\alpha = -2.35$ is assumed (similar to the Kroupa slope for massive stars), then the rate increases to 103^{+110}_{-63} Gpc^{-3} yr^{-1}, which cannot be explained fully by the present analysis (though we note that this estimate may be biased by the chosen upper-mass limit on BHs; Fishbach & Holz 2017).

A full exploration of the many possible combinations of BBH formation channels with self-consistent physics is beyond the scope of this Letter. However, we can ask how three different BBH formation channels can combine to produce the observed LIGO/Virgo BBH merger rate. For BBH mergers produced by the secular interactions with a third companion (the triples channel) we adopt the standard merger rates from Rodriguez & Antonini (2018). For BBH mergers via the classical common-envelope channel, we adopt the standard BBH merger rate from Belczynski et al. (2016). Rather than use multiple different realizations of the common-envelope channel, we adjust the overall normalization of the field BBH merger rate to whatever value would be required to fully explain the observed LIGO/Virgo merger rate (i.e., $\mathcal{R}_{\rm field} = \mathcal{R}_{\rm LIGO/Virgo} - \mathcal{R}_{\rm GC} - \mathcal{R}_{\rm triples}$ at $z < 0.1$)[4] We show these scenarios in Figure 4.

The standard dynamical assumptions produce a merger rate for GCs and field triples of 26 Gpc^{-3} yr^{-1} in the local universe ($z < 0.1$). If the log-uniform BH mass distribution is assumed to be the correct underlying distribution, then these three

[4] Of course, we could have chosen any channel as the free parameter to yield the full LIGO/Virgo rate. We have used the field channel for this purpose because it can potentially explain either all or none of the observed merger rate.

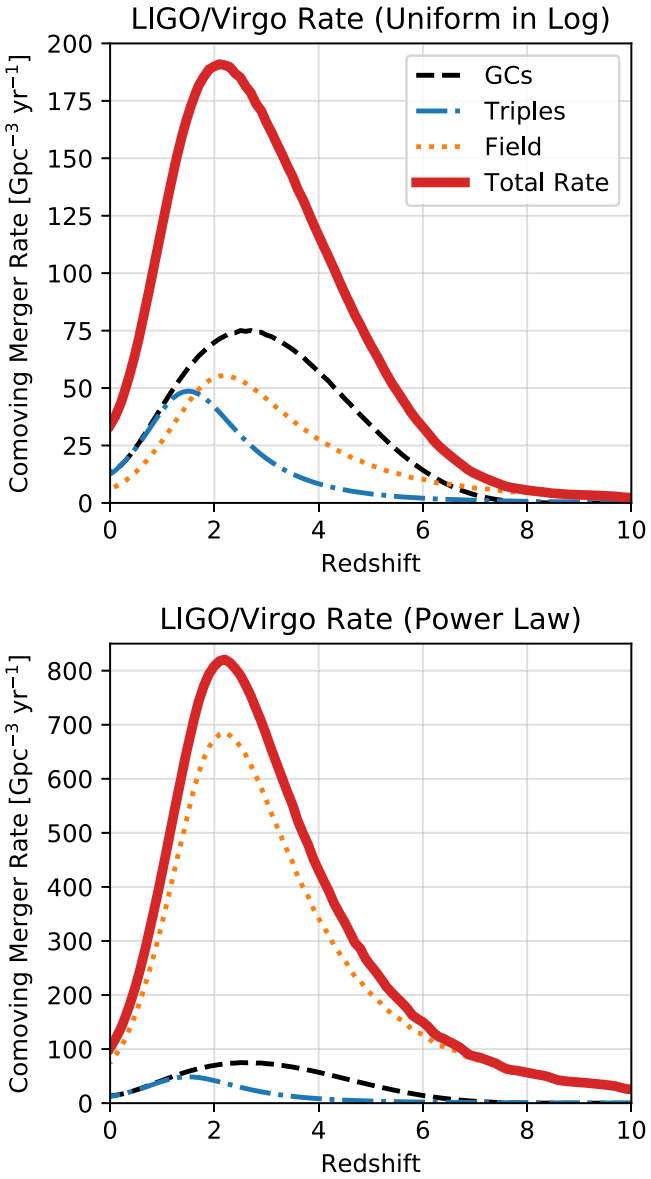

Figure 4. Two examples of BBH merger scenarios, designed to reproduce the observed LIGO/Virgo merger rates (assuming a BH mass distribution either uniform in the logarithm or following a power law with a −2.35 index). We show three different BBH formation channels: GCs, common-envelope evolution (the field, taken from Belczynski et al. 2016), and mergers from field triples (from Rodriguez & Antonini 2018). In each case, the contribution from field binaries is adjusted to complete the observed LIGO/Virgo rate.

channels operate at approximately equal levels, with GCs contributing almost half of all mergers. On the other hand, if the power-law mass function is assumed to be the correct distribution, then GCs contribute approximately one out of every seven BBH mergers in the local universe (while triples contribute one out of every nine).

We emphasize that the merger rates presented in Figure 4 represent only two possible scenarios, and that we have explicitly assumed that the merger rate from GCs and from field triples are known. In reality, we have shown that the rate from GCs can easily span from 4 to 18 Gpc^{-3} yr^{-1} in the local universe (while the rate from triples is even less constrained). This range may expand even further when a realistic distribution of GC initial radii is employed (e.g., Choksi et al. 2018). For the log-uniform rate, this would imply that clusters may contribute anywhere from ∼1/8 to more than half of the observed BBH merger events, while the power-law rate would imply anywhere from 1/25th to 1/5th of BBHs are formed in GCs. In reality, each of these channels contains significant systematic uncertainties, which are often correlated (e.g., the BH natal kicks, which can dramatically effect the rates from all three formation scenarios).

Table 1
Maximum Merger Rate (Observable by Third-generation Detectors) and the Rate at $z = 1$ (Observable by LIGO/Virgo) Normalized by the Merger Rate in the Local Universe for the Contribution from GCs, as well as the Field and Triple Channels

Model	$\mathcal{R}(z_{\rm max})/\mathcal{R}(0)$	$\mathcal{R}(1)/\mathcal{R}(0)$	$z_{\rm max}$
GCs (both r_v)	5.5	3.1	2.7
In-cluster	8.8	4.1	2.9
Ejected	3.5	2.4	2.3
GCs ($r_v = 1$ pc)	6.7	3.5	2.7
In-cluster	10.2	4.5	2.9
Ejected	4.3	2.8	2.5
GCs ($r_v = 2$ pc)	4.0	2.6	2.5
In-cluster	6.8	3.6	2.7
Ejected	2.5	2.0	2.0
Triples	3.9	3.2	1.5
Field	9.2	4.5	2.2

5. Discussion and Conclusion

The most interesting aspect of the results presented in Section 4 is that the peaks (and relative heights) of the merger rates from the different channels are unique. This is hardly surprising, as the three physical mechanisms are expected to produce radically different delay time distributions. In Table 1, we list the maximum of each merger rate and the rate at redshift $z = 1$, normalized to the rate in the local universe. Of all the merger rates analyzed here, the in-cluster merger rates peak earliest, at redshift 2.9, while triple-driven mergers peak latest, at redshift 1.5. Proposed third-generation detectors, such as LIGO Voyager or Cosmic Explorer (Hild et al. 2011; Abbott et al. 2017a) will be able to measure BBH mergers out to redshifts beyond 10. At the same time, it has been shown that LIGO/Virgo may be able to measure the evolution of the BBH merger rate out to $z \sim 1$, and that this information may allow direct measurement of the BBH delay times within 2–5 years (Fishbach et al. 2018). Although the growth in the GC and field rates are identical, the growth between the in-cluster or ejected mergers are significantly different, and may allow these channels to be distinguished by comparing detailed predictions for the masses and eccentricities of in-cluster and ejected BBH mergers from GCs.

Our results show a moderate enhancement over our (Rodriguez et al. 2016a) previous estimates for the merger rate, which bracketed the rate between 2 and 20 Gpc^{-3} yr^{-1}, with a typical value of 5. This increase arises from two factors: first, our newest models (Rodriguez et al. 2018) include full post-Newtonian physics for BBH encounters inside the cluster, yielding a nearly 25% increase in the merger rate, and a significant number of in-cluster mergers that were not present in previous studies (Askar et al. 2016; Rodriguez et al. 2016a; Fragione & Kocsis 2018; Hong et al. 2018). Second, our spatial

density of GCs at high redshifts is somewhat larger than the assumed constant $\rho_{\rm GC} = 0.77\,{\rm Mpc}^{-3}$ in Rodriguez et al. (2015). This is because many GCs have disrupted before the present day, which was not accounted for there. While low-mass GCs do not contribute significantly, the massive clusters can play a significant roll, as any ejected BBHs can merge well after the destruction of their parent clusters.

Our results are mostly consistent with (if slightly higher than) similar studies by Fragione & Kocsis (2018) and Hong et al. (2018). However, we note that the former models all GC formation as occurring instantaneously at $z = 3$, while the latter uses GC models that do not include any in-cluster mergers or post-Newtonian effects. While this study was being finalized, we were informed of a similar work by Choksi et al. (2018), which coupled the semi-analytic model for BBH mergers from Antonini & Rasio (2016) to a detailed model of GC formation and disruption. Although their GC models incorporate less physics than those presented here, this semi-analytic treatment allows for a complete exploration of the parameter space for GC formation and its implication for the BBH merger rate. This includes the initial virial radii of clusters, which we have not analyzed in significant detail due to computational constraints. When a similar distribution for GC effective radii is assumed, they find good agreement between our results and the ones presented here.

We thank Kareem El-Badry and Nick Choksi for useful discussions. C.R. acknowledges support from the Pappalardo Fellowship in Physics at MIT. This work was supported in part by the black hole Initiative at Harvard University, which is funded by the JTF Foundation.

Appendix A
GC Formation Fits

For our fits to Figure 5 from El-Badry et al. (2018), we require an analytic approximation to the cluster formation rate per year in different halo masses as a function of redshift. This essentially forms the cosmological part of our computation, and takes the form of

$$\left.\frac{\dot{M}_{\rm GC}}{d\log_{10}M_{\rm Halo}}\right|_{z(\tau)} \tag{4}$$

in units of $M_\odot\,{\rm yr}^{-1}\,{\rm Mpc}^{-3}$. We find that a log-normal distribution of the form

$$\left.\frac{\dot{M}_{\rm GC}}{d\log_{10}M_{\rm Halo}}\right|_{z} \approx \frac{A(z)}{\sqrt{2\pi}\,\sigma(z)} \times \exp\left(-\frac{\log_{10}M_{\rm halo} - \mu(z)}{2\sigma(z)^2}\right) \tag{5}$$

where $A(z)$, $\mu(z)$, and $\sigma(z)$ are fitted polynomials in the redshift z, fits their results well. We show the original data from El-Badry et al. (2018) and our phenomenological fits in Figure 5.

As stated in the main text, we multiply Equation (5) by an additional factor of 2.6 to account for cluster disruption. The default model of El-Badry et al. (2018) does not include any mechanism for cluster disruption, and was designed primarily to reproduce the observed properties and halo mass/GC mass relationships observed in the local universe. Of course, this meant that their model would unrealistically allow GCs with masses as low as $10^5\,M_\odot$ to survive to the present day. To account for this, the authors applied the cluster disruption model of Choksi et al. (2018) to their model. They found that to reproduce the observed GC mass/halo mass relationship in the local universe, they were required to increase their total GC formation rate by a factor of 2.6 (see El-Badry et al. 2018, Appendix D).

Appendix B
Rate Fit

To generate our expression for $R(r_v, M_{\rm GC}, t)$, we use the GC models created in Rodriguez et al. (2018). These models, created with the state-of-the-art Cluster Monte Carlo (CMC) code (Joshi et al. 2000; Pattabiraman et al. 2013), contain all of the necessary physics to model the formation of merging compact objects, including detailed stellar evolution (Hurley et al. 2000, 2002), dynamical formation of binaries from three isolated BHs (Morscher et al. 2013), and dynamical encounters between binaries and other single/binary stars (Fregeau et al. 2004). Recently, we have upgraded CMC to include fully post-Newtonian dynamics for BHs, including GW emission for isolated binaries and during binary-single and binary-binary encounters (Rodriguez et al. 2018). This has greatly enhanced the number of BBH mergers that can occur in the cluster[5], a significant deviation over previous results (e.g., Askar et al. 2016; Rodriguez et al. 2016a).

To fit the rate to each model, we count the number of mergers that occur in 1 Gyr bins in each model of a given $M_{\rm GC}$. Equation (2) is then assumed to be the time-dependent rate for a Poisson process, giving the probability of observing a certain number of mergers in a bin of width T at a given time t from a cluster with initial mass mass $M_{\rm GC}$ as

$$P(N|R(t, M_{\rm GC}, \theta), T) = e^{-R(t,M_{\rm GC},\theta)T}\frac{(R(t, M_{\rm GC}, \theta)T)^N}{N!} \tag{6}$$

where θ are the five adjustable parameters for Equation (2).

Using the binned merger rate from our GC models, the likelihood for an observed merger rate given our model rate R can be expressed as

$$\mathcal{L}(N|M_{\rm GC}, t, \theta) \propto \prod_i P(N^i|R(t^i, M^i_{\rm GC}, \theta), T) \tag{7}$$

where N^i, t^i, and $M^i_{\rm GC}$ are the number of mergers in the bin of width T at time t from a GC of mass $M_{\rm GC}$. The expression for the probability of θ is simply

$$p(\theta|N, M_{\rm GC}, t, T) \propto \mathcal{L}(N|M_{\rm GC}, t, T, \theta) \times p(\theta) \tag{8}$$

where $p(\theta)$ is the prior probability on the parameters θ. We use a flat prior in the range

$$AM^2_{\rm GC} + BM_{\rm GC} + C > 0$$
$$-\gamma - \gamma_m \log_{10} M_{GC} < 0$$

for all $M_{\rm GC}$ between 10^5 and $10^7\,M_\odot$. Using the `Emcee` package (Foreman-Mackey et al. 2013), we fit the four sets of

[5] These models are nearly identical to those presented in Rodriguez et al. (2018). However, an error in the relativistic physics during BH-BBH scatterings was discovered that reduced the number of in-cluster mergers presented in that work. We still find that $\sim 1/2$ of all BBH mergers occur inside the cluster, but this number reduces to $\sim 1/3$ in the local ($z < 1$) universe. This does not significantly change the results quoted in that paper, but was sufficient to require the generation of new models.

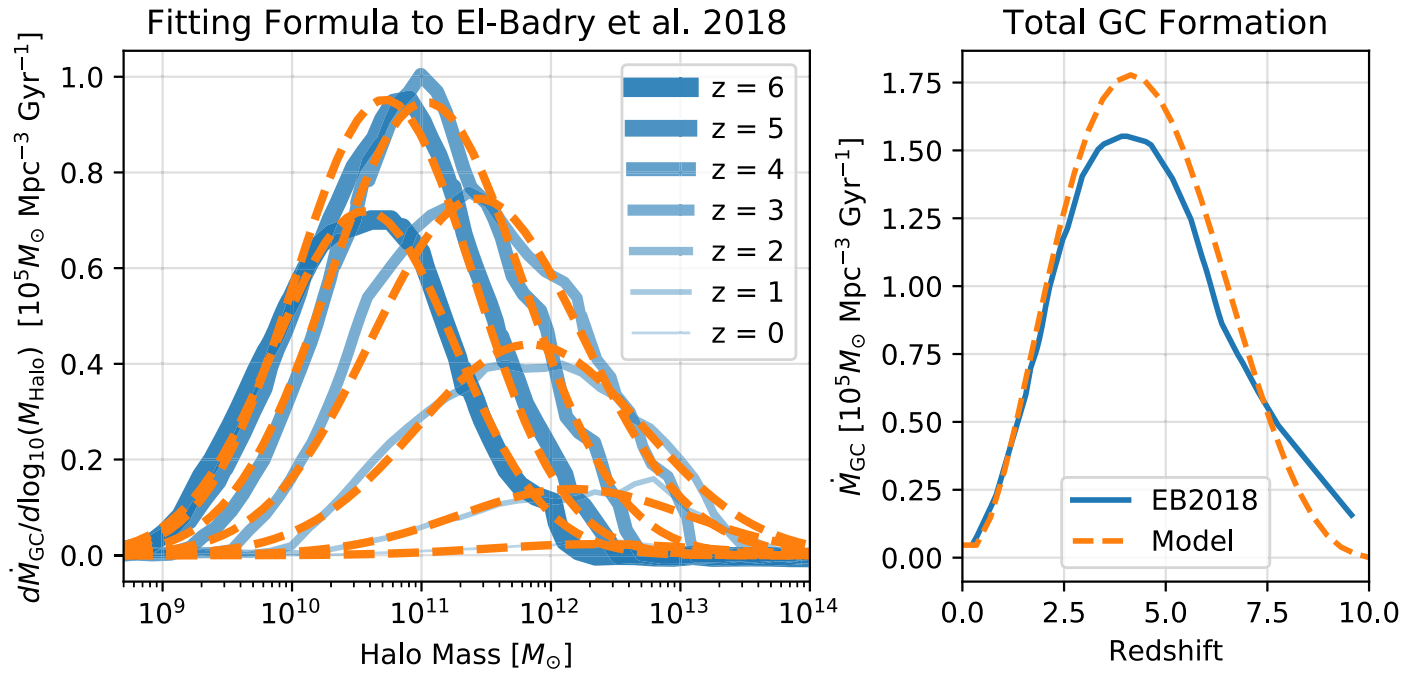

Figure 5. Mass forming in GCs as a function of halo mass at different redshifts. On the left, we show the original plot from El-Badry et al. (2018), as well as our phenomenological fit in Equation (5). The right shows the total GC formation rate as a function of redshift (found by integrating our fit over all halo masses), compared to the same quantity from El-Badry et al. (2018). We find that our predicted density of GCs in the local universe to be in good agreement when integrated over cosmic time ($5.8 \times 10^5\ M_\odot$ Mpc^{-3} in our fit, vs. $5 \times 10^5\ M_\odot$ Mpc^{-3} in the original model).

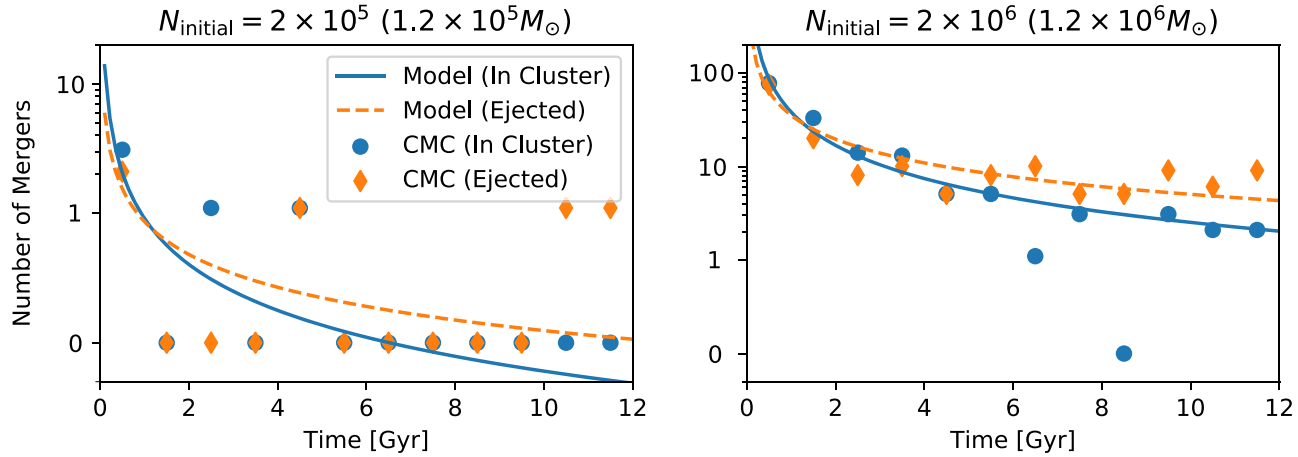

Figure 6. Fit from Equation (2) compared to the binned number of BBH mergers from two GC models Rodriguez et al. (2018). We show two models with initial particle numbers of 2×10^5 and 2×10^6.

merger rates (in-cluster versus ejected and 1 pc verses 2 pc) by minimizing the logarithm of Equation (8). This produces a set of four θ vectors for our rate fitting. The overall merger rate for clusters with a given virial radius is simply the sum of the in-cluster and ejected rates.

As an example, we show the in-cluster and ejected mergers from two models with $r_v = 1$ pc in Figure 6. We find that this function reproduces well both the time-dependent merger rate and the variation with cluster mass for all of our GC models. However, we also note that our rate function (2) goes to infinity as $t \to 0$. In reality, the time required for mass segregation and the formation of BBHs means that the first mergers often do not occur until 100 Myr after cluster formation. To account for this, we simply assume that (2) goes to zero when $t < 100$ Myr. This increases the fidelity of our fit at early times. We also found that the 100 Myr cutoff reduces the number of total mergers for each GC (found by integrating (2) over time from 0 to 12 Gyr) to values that agree well with our CMC models. We do note that this model may over-predict the merger rate from the most massive GCs, because our fits predict that a $10^7\ M_\odot$ GC may produce $\sim 10^4$ mergers over 12 Gyr (in contrast to other semi-analytic techniques, e.g., Antonini & Rasio 2016, where the number is closer to a few times 10^3). However, our CIMF largely disfavors the contribution from such large clusters. We explore the implications of this in Section 3.

ORCID iDs

Carl L. Rodriguez https://orcid.org/0000-0003-4175-8881
Abraham Loeb https://orcid.org/0000-0003-4330-287X

References

Abbott, B. P., Abbott, R., Abbott, T. D., et al. 2016a, PhRvL, 116, 241103
Abbott, B. P., Abbott, R., Abbott, T. D., et al. 2016b, PhRvL, 116, 061102
Abbott, B. P., Abbott, R., Abbott, T. D., et al. 2017a, CQGra, 34, 044011
Abbott, B. P., Abbott, R., Abbott, T. D., et al. 2017b, PhRvL, 118, 221101
Abbott, B. P., Abbott, R., Abbott, T. D., et al. 2017c, PhRvL, 119, 141101
Abbott, B. P., Abbott, R., Abbott, T. D., et al. 2017d, ApJL, 851, L35
Ade, P. A. R., Aghanim, N., Arnaud, M., et al. 2016, A&A, 594, A13
Antonini, F., Chatterjee, S., Rodriguez, C. L., et al. 2016, ApJ, 816, 65
Antonini, F., & Perets, H. B. 2012, ApJ, 757, 27
Antonini, F., & Rasio, F. A. 2016, ApJ, 231, 187
Antonini, F., Toonen, S., & Hamers, A. S. 2017, ApJ, 841, 77
Askar, A., Szkudlarek, M., Gondek-Rosińska, D., Giersz, M., & Bulik, T. 2016, MNRAS, 464, L36
Bae, Y.-B., Kim, C., & Lee, H. M. 2014, MNRAS, 440, 2714
Banerjee, S. 2017, MNRAS, 467, 524
Banerjee, S., Baumgardt, H., & Kroupa, P. 2010, MNRAS, 402, 371
Bastian, N. 2008, MNRAS, 390, 759
Belczynski, K., Dominik, M., Bulik, T., et al. 2010, ApJL, 715, L138
Belczynski, K., Holz, D. E., Bulik, T., & O'Shaughnessy, R. 2016, Natur, 534, 512
Belczynski, K., Kalogera, V., & Bulik, T. 2002, ApJ, 572, 407
Bell, E. F., McIntosh, D. H., Katz, N., & Weinberg, M. D. 2003, ApJSS, 149, 289
Choksi, N., Gnedin, O., & Li, H. 2018, MNRAS, 480, 2343
Choksi, N., Volonteri, M., Colpi, M., et al. 2018, arXiv:1809.01164
Dominik, M., Belczynski, K., Fryer, C., et al. 2012, ApJ, 759, 52
Dominik, M., Belczynski, K., Fryer, C., et al. 2013, ApJ, 779, 72
Dominik, M., Berti, E., O'Shaughnessy, R., et al. 2015, ApJ, 806, 263
Downing, J. M. B., Benacquista, M. J., Giersz, M., & Spurzem, R. 2010, MNRAS, 407, 1946
Downing, J. M. B., Benacquista, M. J., Giersz, M., & Spurzem, R. 2011, MNRAS, 416, 133
El-Badry, K., Quataert, E., Weisz, D. R., Choksi, N., & Boylan-Kolchin, M. 2018, MNRAS, submitted (arXiv:1805.03652)
Fishbach, M., & Holz, D. E. 2017, ApJL, 851, L25
Fishbach, M., Holz, D. E., & Farr, W. M. 2018, ApJL, 863, L41
Foreman-Mackey, D., Hogg, D. W., Lang, D., & Goodman, J. 2013, PASP, 125, 306
Fragione, G., & Kocsis, B. 2018, PhRvL, submitted (arXiv:1806.02351)
Fregeau, J. M., Cheung, P., Portegies Zwart, S. F., & Rasio, F. A. 2004, MNRAS, 352, 1
Gieles, M., Zwart, S. F. P., Baumgardt, H., et al. 2006, MNRAS, 371, 793
Giesler, M., Clausen, D., & Ott, C. D. 2018, MNRAS, 477, 1853
Gnedin, O. Y., & Ostriker, J. P. 1997, ApJ, 474, 223
Harris, W. E., Morningstar, W., Gnedin, O. Y., et al. 2014, ApJ, 797, 128
Hild, S., Abernathy, M., Acernese, F., et al. 2011, CQGra, 28, 094013
Hoang, B.-M., Naoz, S., Kocsis, B., Rasio, F. A., & Dosopoulou, F. 2018, ApJ, 856, 140
Hong, J., Vesperini, E., Askar, A., et al. 2018, MNRAS, 480, 5645
Hurley, J. R., Pols, O. R., & Tout, C. A. 2000, MNRAS, 315, 543
Hurley, J. R., Tout, C. A., & Pols, O. R. 2002, MNRAS, 329, 897
Joshi, K. J., Rasio, F. A., Zwart, S. P., & Portegies Zwart, S. 2000, ApJ, 540, 969
Kremer, K., Chatterjee, S., Ye, C. S., Rodriguez, C. L., & Rasio, F. A. 2018, arXiv:1808.02204
Larsen, S. S. 2009, A&A, 494, 539
Leigh, N. W. C., Geller, A. M., McKernan, B., et al. 2018, MNRAS, 474, 5672
Moody, K., & Sigurdsson, S. 2009, ApJ, 690, 1370
Morscher, M., Pattabiraman, B., Rodriguez, C., Rasio, F. A., & Umbreit, S. 2015, ApJ, 800, 9
Morscher, M., Umbreit, S., Farr, W. M., & Rasio, F. A. 2013, ApJL, 763, L15
O'Leary, R., O'Shaughnessy, R., & Rasio, F. 2007, PhRvD, 76, 061504
O'Leary, R. M., Rasio, F. A., Fregeau, J. M., Ivanova, N., & O'Shaughnessy, R. 2006, ApJ, 637, 937
Pattabiraman, B., Umbreit, S., Liao, W.-k., et al. 2013, ApJS, 204, 15
Petrovich, C., & Antonini, F. 2017, ApJ, 846, 146
Podsiadlowski, P., Rappaport, S., & Han, Z. 2003, MNRAS, 341, 385
Portegies Zwart, S. F., McMillan, S. L., & Gieles, M. 2010, ARA&A, 48, 431
Portegies Zwart, S. F., & Mcmillan, S. L. W. 2000, ApJ, 528, 17
Rodriguez, C. L., Amaro-Seoane, P., Chatterjee, S., & Rasio, F. A. 2018, PhRvL, 120, 151101
Rodriguez, C. L., & Antonini, F. 2018, ApJ, 863, 7
Rodriguez, C. L., Chatterjee, S., & Rasio, F. A. 2016a, PhRvD, 93, 084029
Rodriguez, C. L., Haster, C.-J., Chatterjee, S., Kalogera, V., & Rasio, F. A. 2016b, ApJL, 824, L8
Rodriguez, C. L., Morscher, M., Pattabiraman, B., et al. 2015, PhRvL, 115, 051101
Sadowski, A., Belczynski, K., Bulik, T., et al. 2008, ApJ, 676, 1162
Scheepmaker, R. A., Haas, M. R., Gieles, M., et al. 2007, A&A, 469, 925
Silsbee, K., & Tremaine, S. 2017, ApJ, 836, 39
Tanikawa, A. 2013, MNRAS, 435, 1358
VanLandingham, J. H., Miller, M. C., Hamilton, D. P., & Richardson, D. C. 2016, ApJ, 828, 77
Vitale, S., & Farr, W. M. 2018, PhRvL, submitted (arXiv:1808.00901)
Voss, R., & Tauris, T. M. 2003, MNRAS, 342, 1169
Ziosi, B. M., Mapelli, M., Branchesi, M., & Tormen, G. 2014, MNRAS, 441, 3703